Acta Pharmaceutica Sinica B 2025;15(5):2545−2558

Chinese Pharmaceutical Association
Institute of Materia Medica, Chinese Academy of Medical Sciences

Acta Pharmaceutica Sinica B

www.elsevier.com/locate/apsb
www.sciencedirect.com

ORIGINAL ARTICLE

Deubiquitinase USP13 alleviates doxorubicin-induced cardiotoxicity through promoting the autophagy-mediated degradation of STING

Liming Lin[a,b,†], Jibo Han[c,*,†], Diyun Xu[a,b,†], Zimin Fang[a,b], Bozhi Ye[a,b], Jinfu Qian[a], Xue Han[b,d], Julian Min[d], Xiaohong Long[d], Gaojun Wu[a,*], Guang Liang[a,b,d,*]

[a]*Department of Cardiology, the First Affiliated Hospital of Wenzhou Medical University, Wenzhou 325035, China*
[b]*Chemical Biology Research Center, School of Pharmaceutical Sciences, Wenzhou Medical University, Wenzhou 325035, China*
[c]*Department of Cardiology, the Second Affiliated Hospital of Jiaxing University, Jiaxing 314001, China*
[d]*School of Pharmaceutical Sciences, Hangzhou Medical College, Hangzhou 310014, China*

Received 21 May 2024; received in revised form 27 October 2024; accepted 20 December 2024

KEY WORDS

Deubiquitinating enzyme;
USP13;
STING;
Autophagy;
Inflammation;
Doxorubicin;
Cardiomyocyte;
Cardiotoxicity

Abstract Doxorubicin (Dox) is an anthracycline drug widely applied in various malignancies. However, the fatal cardiotoxicity induced by Dox limits its clinical application. Post-transcriptional protein modification *via* ubiquitination/deubiquitination in cardiomyocytes mediates the pathophysiological process in Dox-induced cardiotoxicity (DIC). In this study, we aimed to clarify the regulatory role and mechanism of a deubiquitinating enzyme, ubiquitin-specific peptidase 13 (USP13), in DIC. RNA-seq analysis and experimental examinations identified that cardiomyocyte-derived USP13 positively correlated with DIC. Mice with cardiac-specific deletion of USP13 were subjected to Dox modeling. Adeno-associated virus serotype 9 (AAV9) carrying *cTNT* promoter was constructed to overexpress USP13 in mouse heart tissues. Cardiomyocyte-specific knockout of USP13 exacerbated DIC, while its overexpression mitigated DIC in mice. Mechanistically, USP13 deubiquitinates the stimulator of interferon genes (STING) and promotes the autolysosome-related degradation of STING, subsequently alleviating cardiomyocyte inflammation and death. Our study suggests that USP13 serves a cardioprotective role in DIC and indicates USP13 as a potential therapeutic target for DIC treatment.

*Corresponding authors.
E-mail addresses: wzmcliangguang@163.com (Guang Liang), gaojunwuwyyy@163.com (Gaojun Wu), jibohanjx2y@163.com (Jibo Han).
[†]These authors made equal contributions to this work.
Peer review under the responsibility of Chinese Pharmaceutical Association and Institute of Materia Medica, Chinese Academy of Medical Sciences.

https://doi.org/10.1016/j.apsb.2025.03.051

1. Introduction

Doxorubicin (Dox) is an anthracycline antitumor drug widely used to treat various malignancies, including lymphomas, leukemias, and solid tumors[1]. However, Dox exhibits a selective affinity to the myocardium compared to other tissues. This cardiac affinity results in Dox-induced cardiotoxicity (DIC), which is characterized by arrhythmia, cardiac dysfunction, and eventually congestive heart failure[2]. DIC is an important challenge for cancer patients undergoing Dox-containing anti-cancer treatment[3]. A variety of pathological processes have been reported to be involved in DIC, including oxidative stress, mitochondrial dysfunction, programmed cell death, and inflammation[4]. Although pharmacological treatment of DIC, such as dexrazoxane, has advanced, the prognosis of DIC patients is still poor[5,6]. Thus, it is urgent to find new mechanisms and targets to develop new strategies for the treatment of DIC.

As a type of post-translational modification, ubiquitination/deubiquitination plays a pivotal role in regulating proteasome degradation or other biological processes of substrate proteins[7]. The E3 ligases and deubiquitinating enzymes (DUBs) collaborate to regulate the ubiquitination of substrate reversibly[7]. DUBs are widely involved in signaling pathways and biological processes by removing ubiquitin from the substrates[8]. Recently, emerging evidence suggests that several DUBs may play a crucial role in DIC[9,10]. Wang and colleagues[9] found that Dox increases the expression of USP36 in cardiomyocytes, and USP36 promotes the pathology of DIC *via* enhancing oxidative stress and cardiomyocyte apoptosis. Another DUB, OTUB1, deubiquitinates c-MYC protein to promote cardiomyocyte apoptosis and oxidative stress induced by Dox[10]. Therefore, the DUB family may be used as a potential molecular library for identifying therapeutic targets for DIC.

Ubiquitin-specific peptidase 13 (USP13), which belongs to the USP subfamily of the DUB family, was first discovered in 1998[11]. In structure, USP13 mainly harbors a ZNF domain and a USP domain consisting of two UBA domains and a catalytic domain[12]. In general, the tandem UBA domain of USP13 binds to the ubiquitin of substrates and catalyzes Lys-63/48/27-linked ubiquitin chain hydrolysis[12]. Recently, it has been reported that USP13 plays a multifaceted regulatory role in numerous diseases by controlling the ubiquitination of different substrates, including antagonizing multiple tumors and improving non-alcoholic steatohepatitis[12-14]. These findings underscore the potential of USP13 as a protective therapeutic target, while the function of USP13 in heart disease, particularly DIC, is still unknown.

In this study, we screened the expression profile of DUBs in DIC hearts and found increased USP13 expression in cardiomyocytes. We then explored the relationship and the underlying mechanism between USP13 and DIC. Cardiomyocyte-specific knockout of USP13 exacerbated DIC, whereas USP13 overexpression in cardiomyocytes mitigated DIC in mice. Stimulator of interferon genes (STING) is an important regulator for innate immune response against pathogens *via* recruiting and activating TANK-binding kinase 1 (TBK1), which subsequently raises the expression of inflammatory cytokines[15]. Recent studies have shown the important role of STING in regulating the pathogenesis of DIC, and genetic or pharmacological inhibition of STING activation can effectively reduce Dox-induced cardiac dysfunction[16]. Mechanistically, we have revealed that USP13 deubiquitinates STING and promotes the autolysosome-related degradation of STING, subsequently alleviating cardiomyocyte inflammation and death. Our study suggests that USP13 serves a cardioprotective role in DIC and indicates USP13 as a potential therapeutic target for DIC treatment.

2. Materials and methods

2.1. Reagents

Doxorubicin (Dox, HY-15142) and Bafilomycin A1 (Baf A1, HY-100558) were purchased from MedChemExpress (Monmouth Junction, NJ, USA). Spautin-1 (S7888) was procured from Selleck (Houston, TX, USA). Dox was solubilized in a 0.9% normal saline solution for *in vivo* experiments. Dimethyl sulfoxide was employed to achieve solubility of Dox and Spautin-1 at suitable concentrations for *in vitro* investigations. 0.1% dimethyl sulfoxide was utilized as vehicle control. MG132 (T2154) was acquired from TargetMol (Shanghai, China). EBSS (C0213) was sourced from Beyotime (Shanghai, China).

Antibodies targeting GAPDH (60004-1-IG, 1:1000), USP13 (16840-1-AP, 1:1000 for Western blot and 1:200 for immunofluorescence staining), Flag (20543-1-AP, 1:1000), His (66005-1-IG, 1:1000), HA (81290-1-RR, 1:1000), MYC (16286-1-AP, 1:1000) and LC3B (14600-1-AP, 1:1000) were acquired from Proteintech (Wuhan, China). Antibodies against STING (13647S, 1:1000), p-STING (72971S, 1:1000), TBK1 (3504S, 1:1000), p-TBK1 (5483S, 1:1000) and SQSTM1/p62 (5114S, 1:1000) were purchased from CST (Danvers, MA, USA). Antibodies specific to Alpha-cardiac actin (M1206-1, 1:200 for immunofluorescence staining) and Vimentin (EM0401, 1:200) were obtained from HUABIO (Hangzhou, China).

2.2. Animals

All procedures involving mice experiments were ethically approved by the Institutional Animal Care and Usage Committee of Wenzhou Medical University (wydw2024-0164) and strictly followed National Institutes of Health guidelines (Guide for the Care and Use of Laboratory Animals, USA). Mice were housed in standardized cages under a 12-h light/dark cycle (lights on at 06:00) with food and water freely available. Before the commencement of the studies, the animals underwent a minimum of 2 weeks of acclimatization within the laboratory environment.

USP13flox/flox (USP13 $^{fl/fl}$) mice, *Myh6*-Cre mice, and WT mice of the C57BL/6J were purchased from GemPharmatech (Nanjing, China). Then, cardiomyocyte-specific deletion of USP13 (USP13CKO) was achieved by crossing USP13 $^{fl/fl}$ mice with *Myh6*-Cre mice. Dox group mice received an intraperitoneal injection of 15 mg/kg of Dox (3 times/week for 2 weeks)[17]. The control group mice received the same amount of PBS injection. Cardiotoxicity was assessed at 4 weeks after the Dox injection.

Cardiac-specific overexpression of UPS13 ($USP13^{oe}$) was achieved by the recombinant adeno associated virus serotype 9 (AAV9). AAV9s with cardiac-specific promoter *cTNT* (*cTNTp*−MCS−3Flag−T2A−EGFP, GV571) and *Usp13* cDNA (NM_001013024) were prepared by GeneChem (Shanghai, China). Two weeks after Dox modeling, 100 μL of saline containing 2×10^{11} v.g. AAV9 viruses was injected through the tail vein. The mice were harvested at 6 weeks after Dox injection.

At the end of the experiment, all mice were sacrificed under sodium pentobarbital anesthesia, and blood samples were collected. Cardiac tissues were fixed with 4% paraformaldehyde or frozen with liquid nitrogen. Echocardiographic parameters are provided in Supporting Information Tables S1 and S2.

2.3. Echocardiography

Cardiac function was monitored *via* echocardiography (Sonics Vevo 2100) throughout the Dox model. Specifically, short-axis views of the left ventricle (LV) were acquired using B-mode imaging. Subsequently, left ventricular ejection fraction (LVEF) and fractional shortening (FS) were precisely calculated based on LV end-diastolic and end-systolic dimensions, which were obtained through M-mode ultrasound analysis.

2.4. Single-cell RNA sequencing (scRNA-seq)

Hearts were dissociated into single cells by the dissociation solution. We combined single-cell suspensions from 3 to 4 hearts into one sample. Using the 10 × Chromium platform (10 × Genomics) 3-prime kit (v2), we built a single-cell library. The cDNA amplification, library preparation, sequencing, and data analysis were all performed by LC-BIO technologies Co., Ltd. (Hangzhou, China).

2.5. Histopathological evaluation

Paraffin-embedded sections were used for hematoxylin and eosin (H&E, G1120, Solarbio, Beijing, China) staining and Masson's trichrome (G1340, Solarbio) staining, the former for cardiac histologic analysis and the latter for collagen fiber analysis. To assess the cardiomyocyte area, OCT-embedded frozen sections were stained for 30 min at 37 °C using a 100 nmol/L concentration of Wheat germ agglutinin (WGA) dye solution (GTX01502, Gene Tex, Irvine, CA, USA). To detect cardiomyocyte apoptosis, OCT-embedded frozen slices were stained for 60 min at 37 °C using the reaction mixture of TUNEL following the manufacturer's instructions (C1089, Beyotime). The cellular origin of USP13 in the heart was analyzed by immunofluorescence double staining. OCT-embedded frozen sections were co-incubated with anti-USP13 and anti-vimentin or anti-α-actin overnight, followed by incubation with AlexaFluor488-labeled secondary antibody or TRITC-labeled secondary antibody for 2 h. DAPI was stained to cell nuclei at ambient temperature.

2.6. Enzyme-linked immunosorbent assay

The serum was extracted from blood specimens and subsequently centrifuged at room temperature for 15 min at 1016 × *g* (5247R, FA-45-48-11*, Eppendorf) to facilitate further research. Serum levels of ANP (F10062-96T, Westang, Shanghai, China) and CK-MB (E006-1-1, JianCheng, Nanjing, China) were quantified using commercial ELISA kits, following the manufacturer's instructions.

2.7. Lactate dehydrogenase (LDH) assay

In vitro studies involved the quantification of LDH release into the culture medium using the LDH Assay Kit (C0016, Beyotime). Conversely, *in vivo* investigations assessed LDH levels in mouse serum utilizing the LDH Kit (BC0685, Solarbio).

2.8. Cell culture, viral transductions, and plasmids transfection

NIH/3T3 and HL-1 cells were obtained from the Chinese Academy of Sciences Type Culture Collection (Shanghai, China). Cells were maintained in DMEM (Gibco, Eggenstein, Germany) supplemented with 10% FBS (R223-00, Vazyme, Nanjing, China) as well as 1% streptomycin and penicillin (C100C5, NCM, Suzhou, China). Cultures were maintained in a humidified incubator at 37 °C with 5% CO_2.

Lentiviral particles were generated by co-transfecting lenti-CRISPRv2 plasmids expressing gRNAs, including mSTING-sgRNA: 5′-TACTTGCGGTTGATC TTACC-3′, targeting STING, along with pPAX2 plasmids into HEK293T cells. Following 48 h of transfection, supernatant cultures containing the lentiviruses were harvested. The HL-1 cells were then treated with polybrene at a concentration of 8 μg/mL the day after LP transduction and incubated for 24 h. Puromycin (1 μg/mL) selection was conducted on the cells to isolate STING knockout (STINGKO) HL-1 cells. Negative control cells were treated with an empty vector consisting of lentiCRISPRv2 that does not express any sgRNA.

Gene overexpression in cells was achieved through the transfection of plasmids. Plasmids encoding USP13 (Mouse), USP13−C343A (Mouse), STING (Mouse), P62 (Mouse), HA−Ub (Mouse), HA−K63 (Mouse), and HA−K48 (Mouse) were procured from GeneChem. Transient transfections into NIH/3T3 and HL-1 cells were performed using Lipofectamine 3000 reagent (Invitrogen, Carlsbad, CA, USA), following the manufacturer's instructions.

2.9. Cell viability assay

HL-1 cell viability was assessed using the CCK-8 (CK04, DOJINDO, Kumamoto, Japan). Briefly, a density of 5000 cells per well was inoculated in 96-well plates and subjected to various experimental treatments. After discarding the medium, 100 μL of fresh medium containing a mixture of 90 μL of fresh medium and 10 μL of CCK-8 solution was added to each well, followed by incubation for 1 h. Absorbance was then measured using a microplate spectrophotometer at 450 nm, with a reference wavelength of 650 nm.

2.10. PI and Hoechst double staining in cultured cells

For apoptosis analysis of cells, following treatment of each cell group, propidium iodide (PI) and Hoechst staining solution were added to the cells for 10 min, as per the instructions provided with the PI staining kit (CA1120, Solarbio). Afterward, the cells were imaged under an inverted fluorescence microscope.

2.11. Western blot analysis and co-immunoprecipitation (Co-IP)

Heart tissue and cells were lysed using RIPA lysis buffer (P0013B, Beyotime), and the protein content was quantified using the

colorimetric technique based on Thomas Brilliant Blue. Subsequently, proteins were isolated using SDS−PAGE and transferred onto a PVDF membrane. After blocking the membranes with 5% skim milk for 1.5 h, they were incubated overnight with primary antibodies (1:1000). Following that, membranes were treated for 1 h with secondary antibodies (1:5000) conjugated with HRP. Then, the ECL fluorescence detection kit (P10300, NCM) was utilized by mixing solutions A and B, and the resulting mixture was applied onto the membrane and visualized using a gel imager. The Bio-Rad Image Analysis System was employed for image visualization and analysis.

For Co-IP, cell or tissue lysates were incubated with the specified antibody (1:200) overnight at 4 °C, where a total lysate was used as input control. Subsequently, the lysates were immunoprecipitated using Protein A + G Agarose beads (P2055, Beyotime) at 4 °C for 2−4 h. Following 3 times washes with PBS, the immunoprecipitated samples were subjected to Western blot analysis.

2.12. Co-IP combined with LC−MS/MS analysis

Initially, HL-1 cell lysates, serving as a rich source of cellular proteins, were prepared. Following this, the USP13 antibody was introduced to these lysates to facilitate the formation of complexes with its substrate proteins. IgG served as a negative control to mitigate nonspecific interactions. Subsequently, the protein samples underwent digestion into peptides for LC−MS/MS analysis, conducted by BIOPROFILE (Shanghai, China). Finally, a scoring system, in conjunction with mass spectrometry data, was applied to identify substrate proteins capable of binding to USP13.

2.13. Real-time quantitative PCR (RT-qPCR)

Total RNA was extracted using TRIzol reagent. The isolated RNA was then reverse transcribed into cDNA using the HiScript III All-in-one RT SuperMix Perfect for qPCR kit (R333-01, Vazyme). Using ChamQ Universal SYBR qPCR Master Mix, the cDNA was subsequently subjected to RT-qPCR. Primers in this study (Supporting Information Table S3) were obtained from Sangong Biotech.

2.14. Statistical analyses

Continuous data in this study are presented as mean ± standard error (SEM). Student's *t*-test was employed to compare significant differences between two groups, while ANOVA with Bonferroni's correction for multiple comparisons was utilized to compare more than two data groups. When identifying significant differences *via* ANOVA, we employed Bonferroni's correction for *post hoc* multiple comparisons to pinpoint specific group differences. The statistical analysis was performed in GraphPad Pro Prism 8.0 (GraphPad, San Diego, CA, USA). A significance level of $P < 0.05$ was considered statistically significant for all analyses conducted in this study.

3. Results

3.1. Cardiomyocyte USP13 expression is increased in Dox-induced cardiomyopathy

We first screened the expression of all DUB genes in DIC by analyzing 2 transcriptome sequencing datasets from the GEO database. Elevated USP13 was observed in both Dox-treated mouse heart tissues (GSE23598, Fig. 1A) and cardiac tissues from patients with dilated cardiomyopathy (GSE120895, Fig. 1B). Next, we overexpressed several cardiovascular diseases associated DUBs, including USP25[18], USP28[19], YOD1[20], OTUD1[21], OTUD5[22], OTUD6a[23], and JOSD2[24] in HL-1 cardiomyocytes, and showed that overexpression of USP13, USP25, YOD1, OTUD5, and JOSD2 significantly reduced Dox-induced LDH release in HL-1 cells (Fig. 1C). Through a comparison of transcriptomes and function screen, we identified USP13 as a potential regulator of DIC (Fig. 1D).

Corroborating these findings, both mRNA and protein levels of USP13 were significantly elevated in Dox-induced mouse heart tissues (Fig. 1E and F). Single-cell RNA sequencing data showed the cell distribution of USP13 expression in cardiomyocytes (Fig. 1G, Supporting Information Fig. S1A). Western blot confirmed the expression of USP13 protein in cardiomyocytes rather than non-cardiomyocytes (Fig. 1H, Fig. S1B). Furthermore, a time-dependent upregulation of USP13 protein was observed in Dox-challenged HL-1 cells (Fig. 1I, Fig. S1C). In contrast, Dox treatment did not increase the USP13 level in cardiac fibroblasts (Fig. S1D). Immunofluorescence staining also demonstrated the colocalization of USP13 and α-actin (cardiomyocyte marker) but not vimentin (fibroblast marker) (Fig. 1J, Fig. S1E). Collectively, these results demonstrated that USP13 was predominantly increased in cardiomyocytes under Dox stimulation.

3.2. Cardiomyocyte specific knockout of USP13 exacerbates Dox-induced cardiac dysfunction and injury in vivo

To evaluate the effect of USP13 on Dox-induced cardiac dysfunction and injury, cardiomyocyte-specific USP13 knockout (USP13CKO) mice were applied and subjected to Dox modeling (at 15 mg/kg, 3 times/week for 2 weeks). The successful knockout of USP13 was verified in isolated cardiomyocytes of USP13CKO mice (Supporting Information Fig. S2A). Cardiac dysfunction was assessed at the end of 4 weeks of Dox injection. Echocardiographic evaluation revealed that both $USP13^{fl/fl}$ and USP13CKO mice experienced a significant decrease in ejection fraction (EF) and fractional shortening (FS) after Dox treatment, while these reductions were more pronounced in USP13CKO mice (Fig. 2A and B). Correspondingly, the serum levels of atrial natriuretic peptide (ANP), lactate dehydrogenase (LDH), and creatine kinase-MB (CK-MB) were markedly elevated in response to Dox, which were further increased in the USP13CKO group (Fig. 2C−E). Morphological examinations showed aggravated cardiac atrophy in USP13CKO mice after Dox treatment (Fig. 2F and G, Fig. S2B). Wheat germ agglutinin (WGA) staining confirmed the changing trend in cardiomyocyte atrophy in these four groups (Fig. 2H and I). The collagen deposition (Fig. 2J and K) and fibrosis marker proteins (COL-1/CTGF) (Fig. S2C) in heart tissues were also further enhanced in the Dox-treated USP13CKO group, compared to that in $USP13^{fl/fl}$ + Dox mice. USP13CKO also predisposes cardiomyocytes to cell death after Dox treatment than $USP13^{fl/fl}$ mice (Fig. 2L and M). These data suggest that cardiomyocyte-specific knockout of USP13 exacerbates Dox-induced cardiac injury and dysfunction.

3.3. Cardiomyocyte-specific overexpression of USP13 alleviates cardiac dysfunction and injury induced by Dox

Then, we tested whether cardiomyocyte-specific overexpression of USP13 had a therapeutic effect on established DIC. We constructed AAV9s carrying *cTNT* promoter to over-express USP13

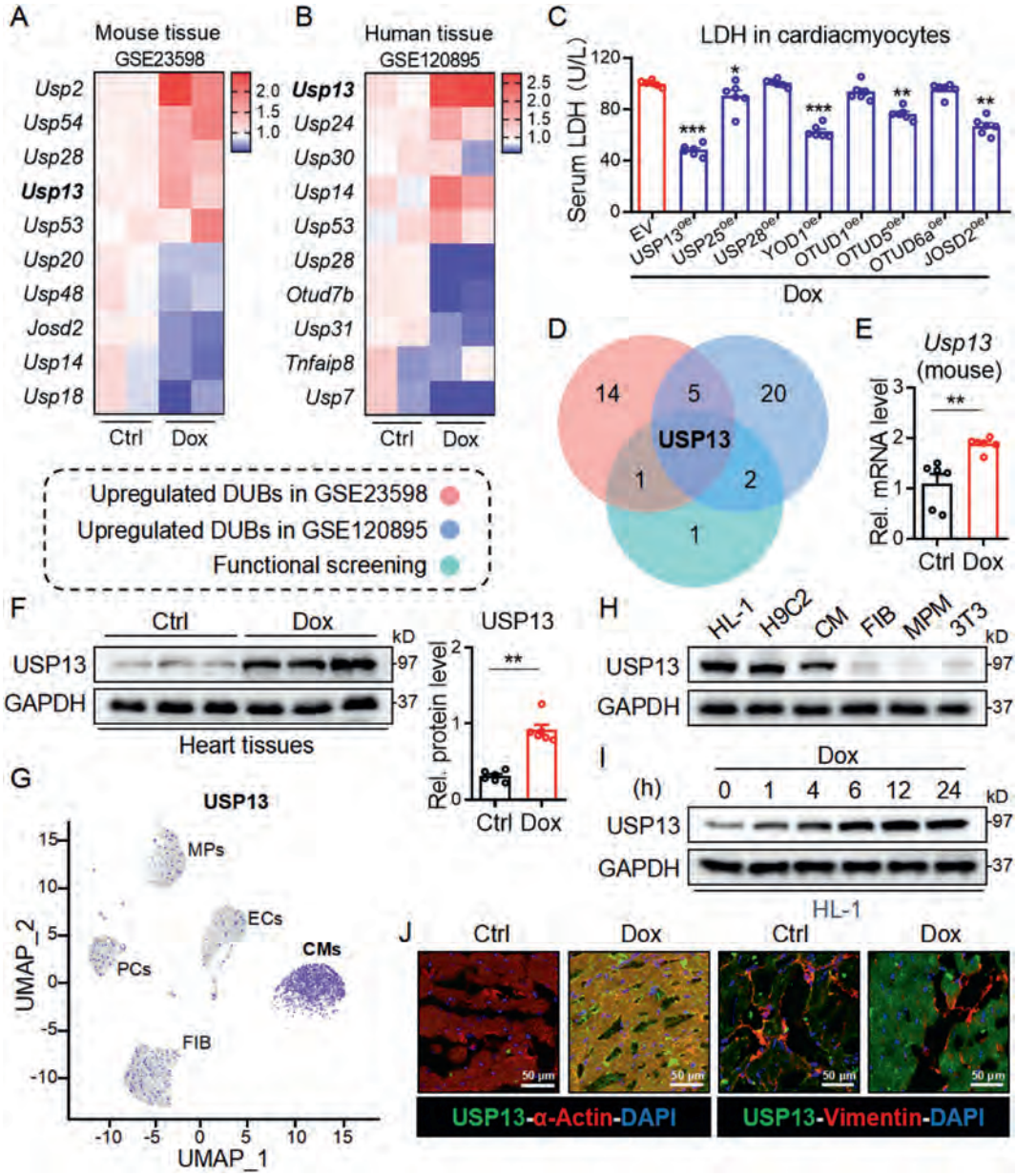

Figure 1 Cardiomyocyte USP13 expression is increased in Dox-induced cardiomyopathy. (A, B) Heatmaps illustrate the DUBs' expression levels in datasets GSE23598 (Dox-induced mouse heart tissues) and GSE120895 (cardiac tissues from patients with dilated cardiomyopathy). (C) The level of lactate dehydrogenase (LDH) in cell supernatants. HL-1 cells were transfected with 8 different DUBs before the addition of Dox (1 μmol/L, 24 h) ($n = 6$). (D) Comprehensive combined GEO database and cell viability analysis for identification of USP13 as a regulator in DIC. Red denotes upregulated DUBs in GSE23598, blue represents upregulated DUBs in GSE120895, and green indicates results from functional screening. (E, F) The mRNA or protein level of USP13 in Dox-induced mice heart tissue ($n = 6$). (G) The single-cell sequencing data reveals the distribution of USP13 in mice heart. (Single-cell suspensions from 3 to 4 hearts were pooled as 1 sample). (H) The protein levels of USP13 in different cells. (I) The protein level of USP13 in HL-1 cells with Dox (1 μmol/L) for 0−24 h. (J) Immunofluorescence staining was performed on heart sections from Dox mice to detect USP13 (green) along with α-actin or vimentin (both red). Merged images indicate co-localization (yellow). Data are presented as mean ± SEM; $^{**}P < 0.01$.

(USP13^{oe}) specifically in cardiomyocytes in mice. Generally, AAV9-mediated protein overexpression occurs 2 weeks after initial AAV9 injection. WT mice were initially subjected to Dox administration, and subsequently injected with AAV9s encoding USP13 or empty vector (EV) at 2 weeks after Dox injection and harvested at 6 weeks after the Dox injection (Fig. 3A). Western blot analysis confirmed the overexpression of USP13 in mouse heart tissues (Fig. 3B). WT mice exposed to Dox exhibited cardiac dysfunction, which was significantly ameliorated by cardiomyocyte-specific USP13^{oe} (Fig. 3C and D). The cardioprotective role of USP13 was further validated by the examination of serum LDH and CK-MB levels (Fig. 3E and F). Morphological and histological evaluations of cardiac tissues showed preservation of structural integrity by USP13^{oe} against

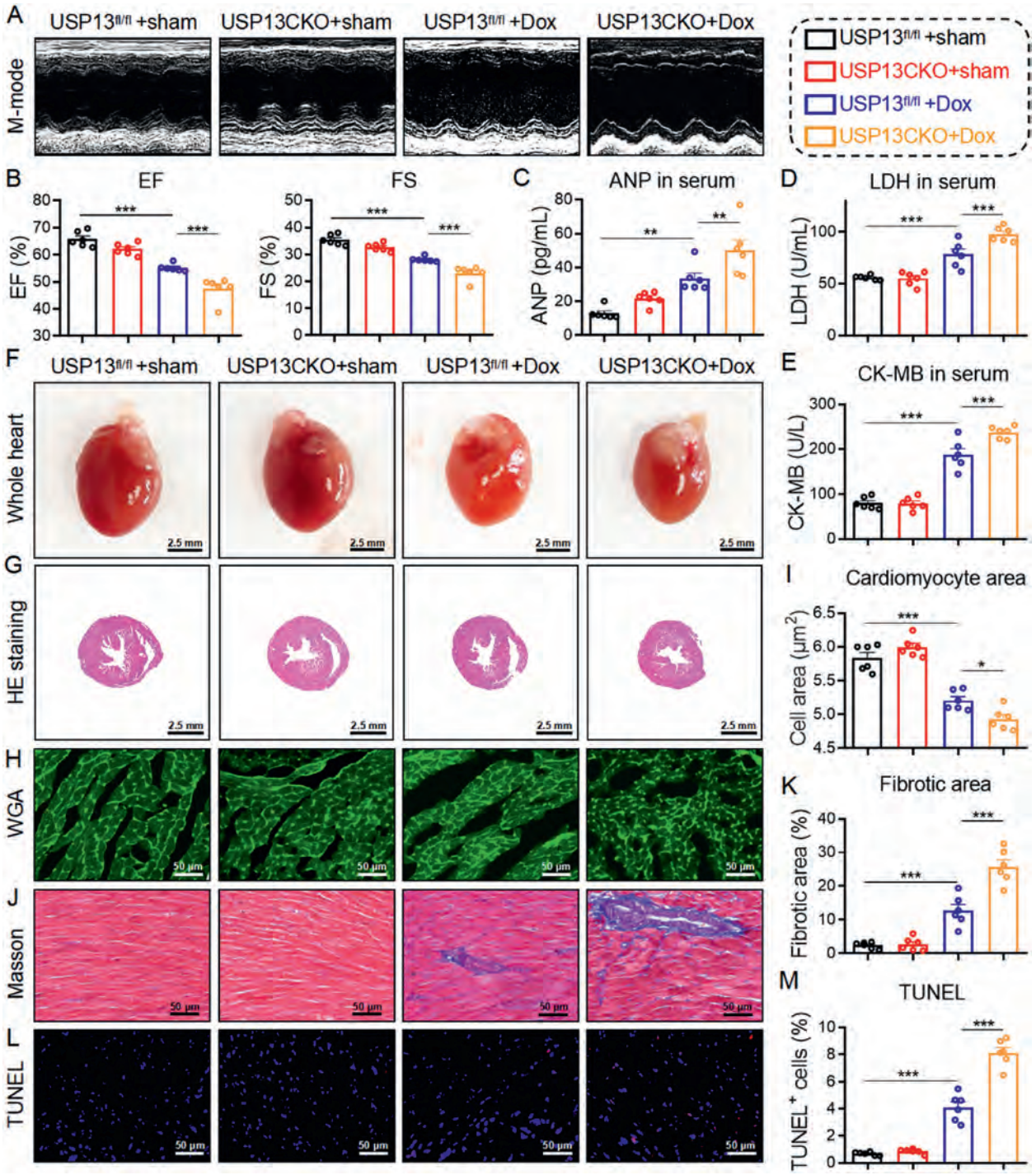

Figure 2 Cardiomyocyte specific knockout of USP13 exacerbates Dox-induced cardiac dysfunction and injury *in vivo*. USP13$^{fl/fl}$ and USP13CKO mice were intraperitoneally injected with either PBS or Dox (15 mg/kg, 3 times/week for 2 weeks). DIC was assessed at 4 weeks after Dox injection. (A) Representative M-mode images of indicated groups. (B) Ejection fraction (EF) and fractional shortening (FS) in different groups ($n = 6$). (C−E) Serum atrial natriuretic peptide (ANP), LDH, and creatine kinase-MB (CK-MB) in different groups ($n = 6$). (F) Whole heart images of indicated groups. (G) HE staining of cardiac sections. (H, I) Representative wheat germ agglutinin (WGA) fluorescence staining images and quantification showing relative cardiomyocyte size ($n = 6$). (J, K) Masson staining of cardiac sections and quantification of collagen ($n = 6$). (L, M) TUNEL staining of cardiac sections and quantification of TUNEL-positive cells ($n = 6$). Data are presented as mean ± SEM; $^*P < 0.05$, $^{**}P < 0.01$, $^{***}P < 0.001$.

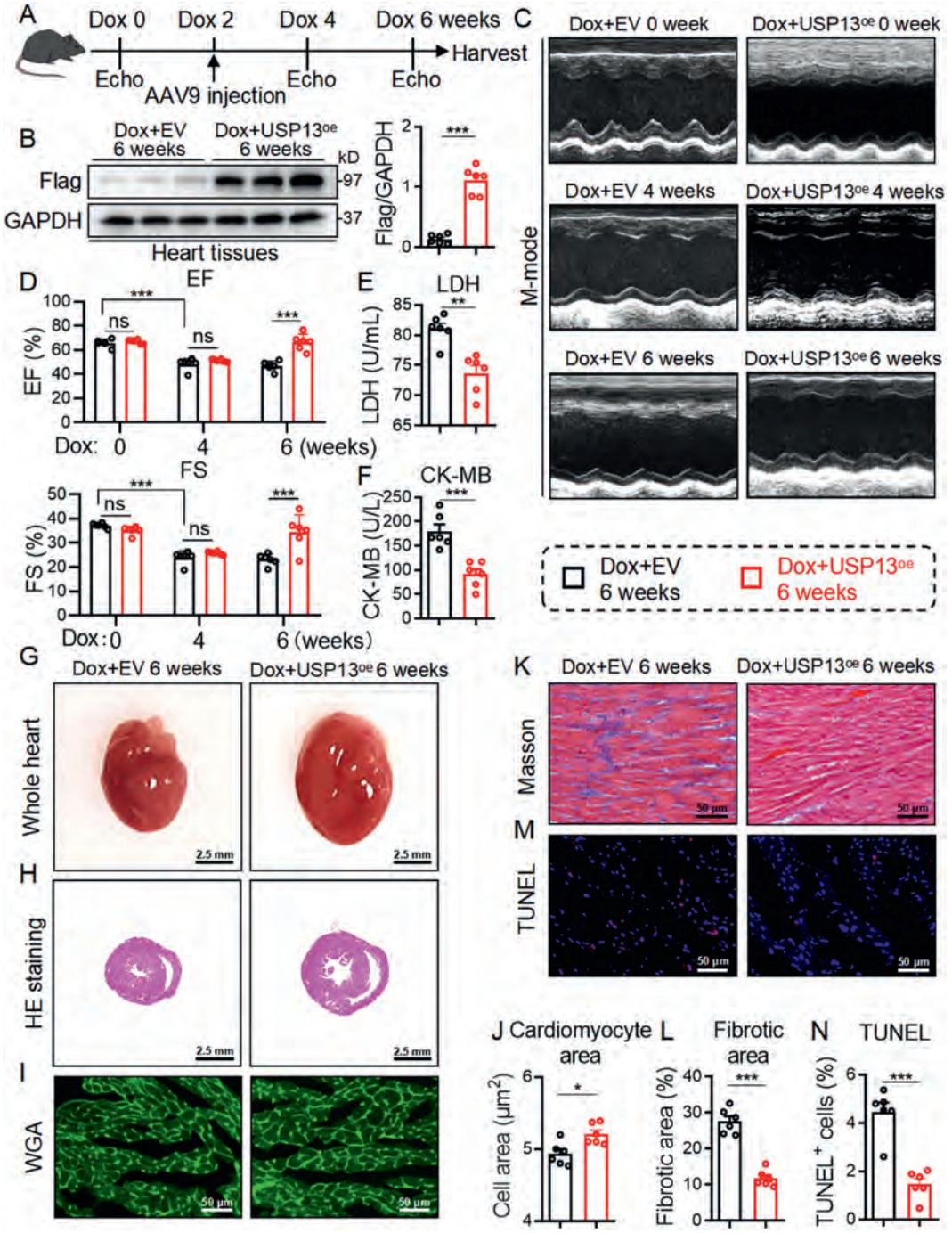

Figure 3 Cardiomyocyte-specific overexpression of USP13 alleviates cardiac dysfunction and injury induced by Dox. (A) Schematic diagram outlining animal experiments: mice were injected with AAV9 viruses (2×10^{11} v.g., 100 μL) after 2 weeks of injection of Dox (15 mg/kg, 3 times/week). The mice were harvested at 6 weeks after Dox injection. (B) Protein level of Flag−USP13 in heart tissues ($n = 6$). (C) Representative M-mode images of indicated groups. (D) EF and FS in different groups ($n = 6$). (E, F) Biochemical analysis of serum LDH, and CK-MB ($n = 6$). (G) Whole heart images of indicated groups. (H) HE staining of cardiac sections. (I, J) Representative WGA fluorescence staining images and quantification showing relative cardiomyocyte size ($n = 6$). (K, L) Masson staining of cardiac sections in heart sections and quantification of collagen ($n = 6$). (M, N) TUNEL staining of cardiac sections and quantification of TUNEL-positive cells ($n = 6$). Data are presented as mean ± SEM; ns = no significance, $^{*}P < 0.05$, $^{**}P < 0.01$, $^{***}P < 0.001$.

Dox treatment (Fig. 3G and H, Supporting Information Fig. S3A). The cardiomyocyte atrophy was also diminished by USP13^{oe} in Dox-induced mice (Fig. 3I and J). Likewise, cardiomyocyte-specific USP13^{oe} significantly ameliorated Dox-induced myocardial fibrosis (Fig. 3K and L) and reduced the expression of fibrosis markers COL-1 and CTGF (Fig. S3B). Moreover, TUNEL assays showed a reduction of cardiomyocyte death in USP13^{oe} mice with Dox injection (Fig. 3M and N). Collectively,

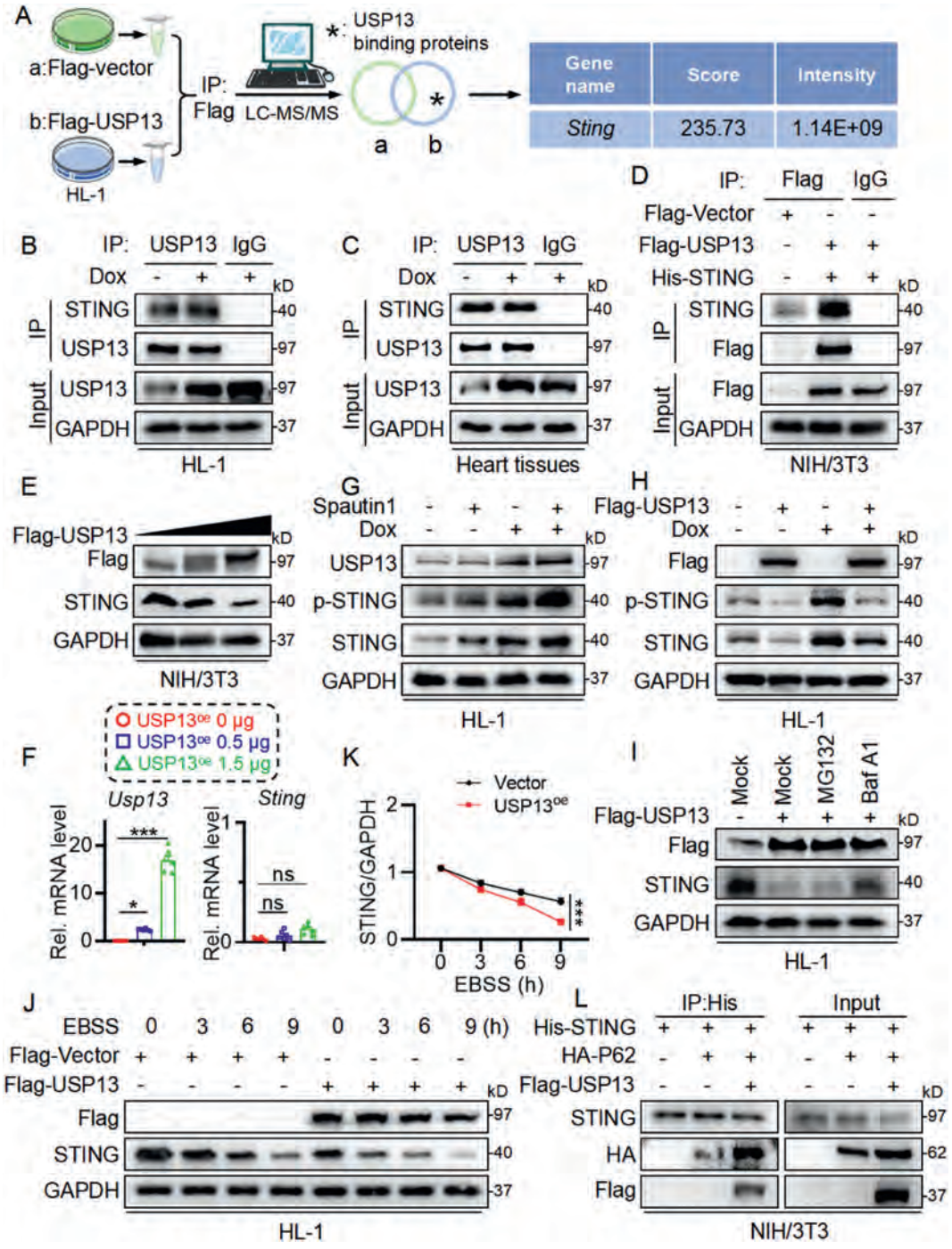

Figure 4 USP13 directly binds to STING and promotes the autophagy-dependent degradation of STING. (A) Schematic representation of the integration of Co-IP with LC−MS/MS for USP13 substrate identification. (B) The Co-IP analysis of USP13 and STING in Dox-treated HL-1 cells (1 μmol/L, 24 h). (C) Co-IP of USP13 and STING in heart tissues upon Dox treatment. (D) Co-IP of USP13 and STING in NIH/3T3 cells co-transfected with Flag−USP13 and His−STING plasmids. (E) Immunoblot of USP13 and STING in NIH/3T3 cells transfected with Flag−USP13. (F) The mRNA levels of *Usp13* and *Sting* in NIH/3T3 cells transfected with Flag−USP13 ($n = 6$). (G) Representative immunoblot images of USP13, p-STING, and STING in HL-1 cells with Spautin-1 (10 μmol/L, 2 h) and then Dox. (H) Representative immunoblot images of USP13, p-STING, and STING in HL-1 cells transfected with Flag−EV or Flag−USP13 plasmids and then Dox stimulation. (I) Representative immunoblot images of Flag−USP13 and STING in HL-1 cells transfected with either Flag−EV or Flag−USP13 plasmids, and subjected to treatment with Mock, MG132 (10 μmol/L), and bafilomycin A1 (Baf A1, 0.2 μmol/L). (J, K) Representative immunoblot images of Flag−USP13 and STING in HL-1 cells transfected with Flag−EV or Flag−USP13 plasmids, and exposed to EBSS for 0, 3, 6, and 9 h (down), quantification of STING (up) ($n = 6$). (L) Co-IP of STING, P62 and Flag−USP13 in NIH/3T3 cells co-transfected with His−STING, HA−P62 and Flag−USP13 plasmids. Data are presented as mean ± SEM; ns, no significance, $^{*}P < 0.05$, $^{***}P < 0.001$.

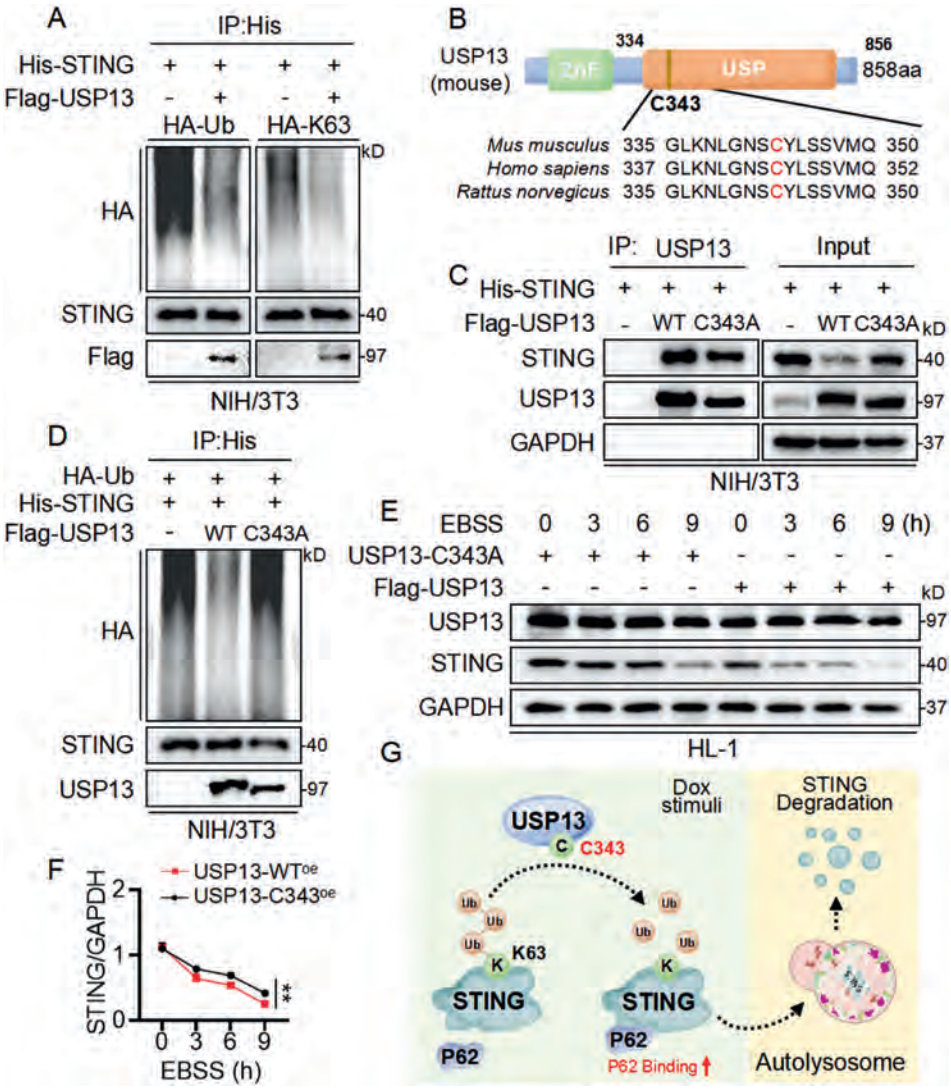

Figure 5 USP13 modulates K63-linked deubiquitination of STING *via* the C343 site. (A) NIH/3T3 cells were co-transfected with His−STING, HA−Ub or HA−K63 along with Flag−USP13, followed by treatment with 0.2 μmol/L Baf A1 for 8 h. Lysates were then subjected to Co-IP with anti-His, followed by immunoblotting with antibodies against HA, STING, and Flag. (B) A schematic illustration depicting the USP13 active site mutation (C343). (C) Co-IP of Flag−USP13 and STING in NIH/3T3 cells co-transfected with Flag−EV, Flag−USP13−WT, Flag−USP13−C343A, and His−STING plasmids. (D) NIH/3T3 cells were transfected with His−STING and HA−Ub along with either Flag−USP13−WT or Flag−USP13−C343A, followed by treatment with 0.2 μmol/L Baf A1 for 8 h. (E, F) Representative immunoblot images of Flag−USP13 and STING in HL-1 cells transfected with either Flag−USP13−WT or Flag−USP13−C343A plasmids, and exposed to EBSS for 0, 3, 6, and 9 h, along with quantification of STING. (G) Illustrative schematic outlines that USP13 regulates K63-linked deubiquitination of STING *via* its active site C343 and subsequently promotes the degradation of STING *via* P62-mediated autophagy. Data are presented as mean ± SEM; $^{**}P < 0.01$.

these results demonstrate the potential of cardiomyocyte USP13 to counteract DIC in mice.

3.4. USP13 directly binds to STING and promotes the autophagy-dependent degradation of STING

As a DUB, USP13 works through directly binding to and then deubiquitinating its substrates. To identify the potential substrates of USP13 in cardiomyocytes, we utilized Co-IP in conjunction with LC−MS/MS analysis. Interestingly, we identified STING as a potential substrate of USP13 in cardiomyocytes (Fig. 4A and Supporting Information Table S4). A recent study has shown the important role of STING in regulating the pathogenesis of DIC, and inhibition of STING activation can effectively reduce Dox-induced cardiac dysfunction[16]. Thus, we hypothesize that USP13 negatively regulates DIC probably through deubiquitinating STING. We first confirmed the endogenous interaction between USP13 and STING proteins in HL-1 cells and cardiac tissues (Fig. 4B and C). Co-IP results further corroborated the exogenous interaction of USP13 and STING in NIH/3T3 cells co-transfected with Flag−USP13 and His−STING (Fig. 4D).

Next, we investigated the impact of USP13 on the stability of STING. Overexpressing USP13 in NIH/3T3 cells resulted in the decrease of STING expression (Fig. 4E and Supporting

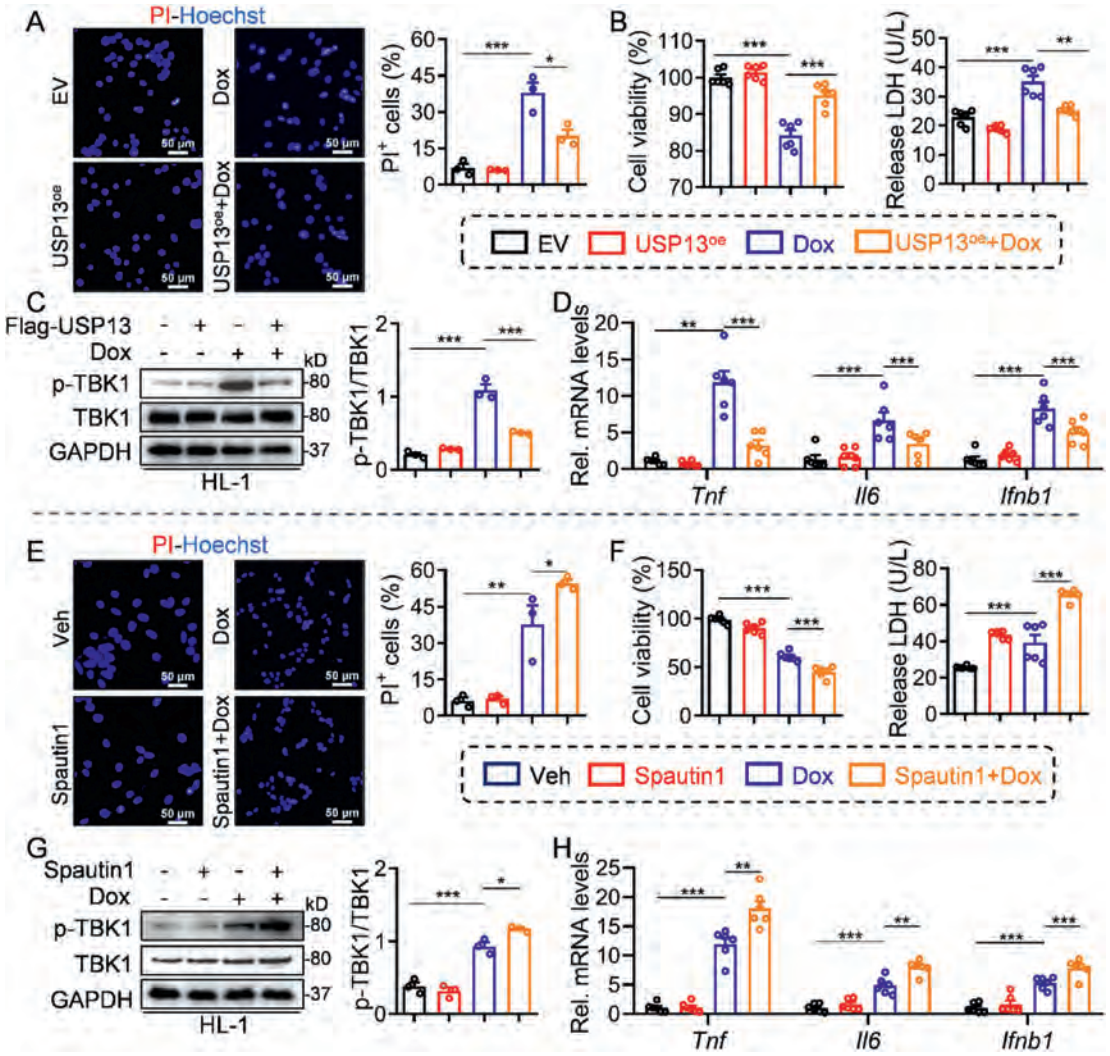

Figure 6 USP13 attenuates Dox-induced cardiomyocyte death and inflammation *via* negatively regulating STING. (A−D) HL-1 cells were transfected with the USP13 plasmid 24 h subsequent to the 1 μmol/L Dox. (A) Representative photographs stained with propidium iodide (PI) and quantitative data for PI positive nuclear ($n = 3$). (B) The release of LDH and cell viability in cells ($n = 6$). (C) Representative immunoblot images of p-TBK1 and TBK1, along with quantification of p-TBK1/TBK1 ($n = 6$). (D) The mRNA levels of *Tnf*, *Il6*, and *Ifnb1* in each group ($n = 6$). (E−H) HL-1 cells were treated with the Spautin-1 2 h before exposure to 1 μmol/L Dox. (E) Representative photographs stained with PI and quantitative data for PI positive nuclear ($n = 3$). (F) The release of LDH and cell viability in cells ($n = 6$). (G) Representative immunoblot images of p-TBK1 and TBK1, along with quantification of p-TBK1/TBK1 ($n = 6$). (H) The mRNA levels of *Tnf*, *Il6* and *Ifnb1* in each group ($n = 6$). Data are presented as mean ± SEM; $^{*}P < 0.05$, $^{**}P < 0.01$, $^{***}P < 0.001$.

Information Fig. S4A), and this decrease was not due to the transcriptional change of STING (Fig. 4F), implying the presence of a post-transcriptional regulatory mechanism. Subsequently, we pharmacologically inhibited USP13 with a specific inhibitor Spautin-1[25], and showed a similar result that the inhibition of USP13 activity increased STING protein content and phosphorylation (Fig. 4G, Fig. S4B). As expected, USP13 overexpression decreased the STING protein level and the subsequent STING phosphorylation in Dox-induced HL-1 cells (Fig. 4H, Fig. S4C). Further, we applied the protein synthesis inhibitor Cycloheximide (CHX). As shown in Fig. S4D, USP13 decreased the half-life of STING protein in HL-1 cells. These results suggest that USP13 promotes the degradation of STING in cardiomyocytes.

To explore USP13-mediated degradation of STING protein, HL-1 cells expressing Flag−USP13 were subjected to proteasome inhibitors or autophagy inhibitors. As shown in Fig. 4I and Fig. S4E, proteasome inhibitor (MG132) showed no effect on USP13-mediated STING degradation, while autophagy inhibitor (Baf A1) exclusively inhibited the degradation of STING, indicating the involvement of the autophagy−lysosome pathway. Next, we tested the autolysosome-related degradation of STING by using an autophagy inducer EBSS. As expected, the degradation rate of STING was increased in USP13-overexpressing NIH/3T3 cells treated with EBSS (Fig. 4J and K). A recent study reported that P62, a crucial mediator of autophagy, interacted with STING to promote the degradation of STING through autophagy[26]. Thus, we may guess that USP13 promotes the autolysosome-related degradation of STING in a P62-dependent manner. We examined the effect of USP13 on the binding of P62 to STING and showed that USP13 overexpression facilitated the interaction between STING and P62 in NIH/3T3 cells (Fig. 4L), cultured cardiomyocytes (Supporting Information Fig. S5A), and heart tissues (Fig. S5B). It has been

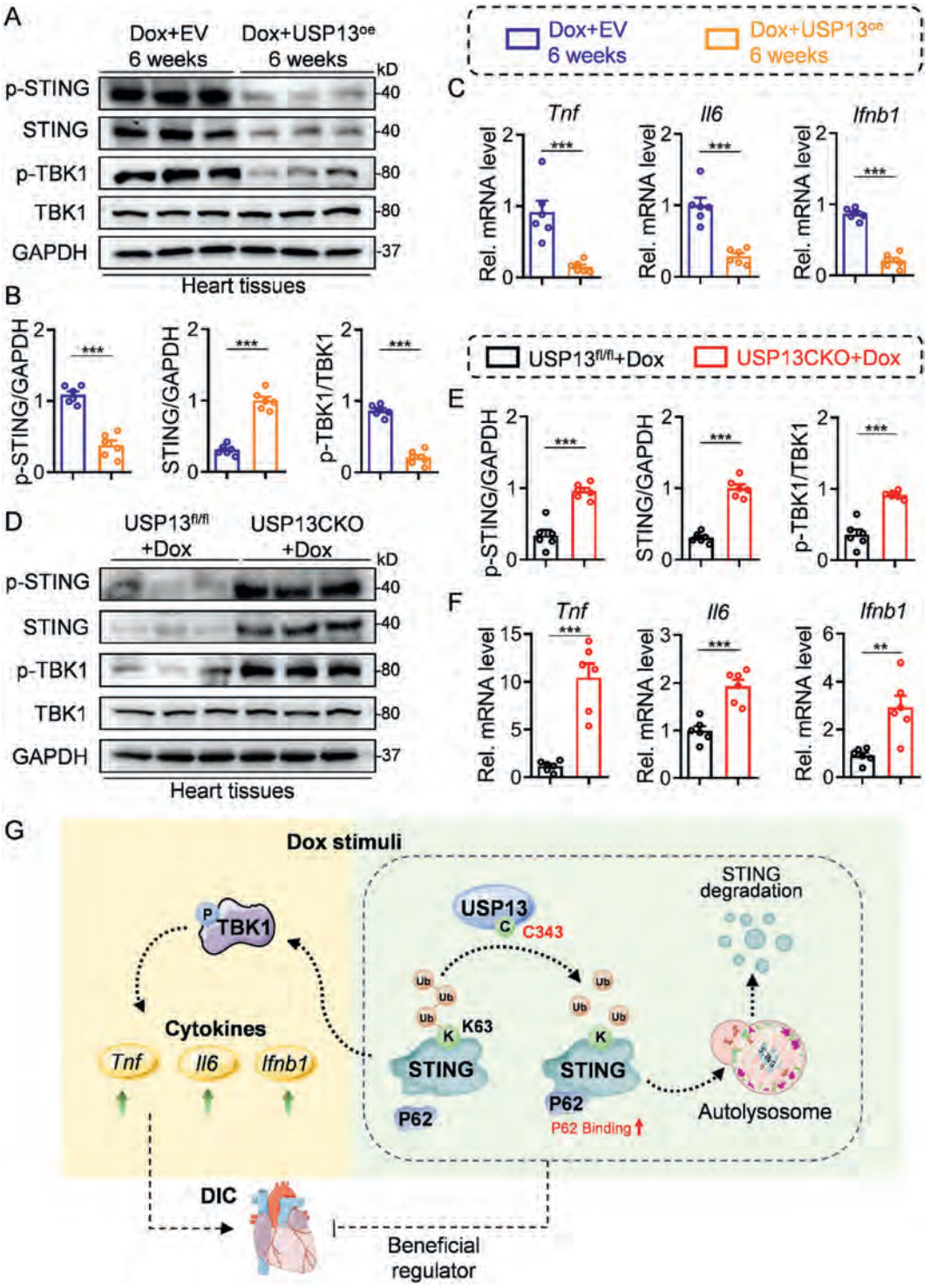

Figure 7 USP13 negatively regulates Dox-induced STING activation and inflammation *in vivo*. (A–C) Mice were injected with AAV9 viruses (2×10^{11} v.g., 100 μL) after 2 weeks of injection of Dox (15 mg/kg, 3 times/week). The mice were harvested at 6 weeks after Dox injection. (A, B) Protein levels of p-STING, STING, p-TBK1, and TBK1 in heart tissue, along with the quantification ($n = 6$). (C) The mRNA levels of *Tnf*, *Il6* and *Ifnb1* ($n = 6$). (D–F) USP13$^{fl/fl}$ and USP13CKO mice were intraperitoneally injected with either PBS or Dox (15 mg/kg, 3 times/week for 2 weeks). Cardiotoxicity was assessed at 4 weeks after Dox injection. (D, E) The protein levels of p-STING, STING, p-TBK1 and TBK1 in heart tissue, along with the quantification ($n = 6$). (F) The mRNA levels of *Tnf*, *Il6* and *Ifnb1* ($n = 6$). (G) The schematic diagram illustrates the principal findings of this study. Data are presented as mean ± SEM; $^{**}P < 0.01$, $^{***}P < 0.001$.

reported that Parkin protects against Dox-induced cardiotoxicity through enhancing mitophagy[27]. Thus, we detected the effect of USP13 on Parkin in cardiomyocytes. As shown in Fig. S5C, USP13 overexpression did not affect the protein level of Parkin in HL-1 cells with or without Dox treatment. Likewise, Co-IP results showed no interaction between USP13 and Parkin in Dox-induced cardiomyocytes (Fig. S5D). These results demonstrated that USP13 directly binds STING and promotes the degradation of STING *via* P62-mediated autophagy.

3.5. USP13 modulates K63-linked deubiquitination of STING via the C343 site

Next, we explored the impact of USP13 on STING deubiquitination. It has been reported that USP13 has no hydrolytic activity to K48 and K63 chain diubiquitin but can slowly hydrolyze K63 chain tetraubiquitin to triubiquitin and monoubiquitin[28]. Co-transfection of NIH/3T3 cells with Flag−USP13, HA−Ub/K63, and His−STING showed that USP13 removed the ubiquitin chain of STING, especially the K63-linked ubiquitin chain (Fig. 5A). In addition, we confirmed that USP13 modulates K63-linked deubiquitination of STING in cultured cardiomyocytes (Supporting Information Fig. S6A). K63-linked ubiquitin chain predominantly affects the protein−protein interaction, suggesting that the K63-linked deubiquitination of STING by USP13 may promote the binding between P62 and STING. As shown in Fig. S6B, USP13^{oe} also decreased the STING ubiquitination in mouse heart tissues. The active site cysteine-343 (C343) in the USP domain of USP13 exhibits evolutionary conservation across different species[29]. Here, we constructed a USP13−C343A mutant (mutation of cysteine at position 343 to alanine) (Fig. 5B), which lacks USP13 deubiquitinase activity. As shown in Fig. 5C, USP13−C343A still binds with STING, same as its wild-type homolog (USP13−WT). However, the USP13−C343A mutant could not remove ubiquitin molecules from STING compared to USP13−WT (Fig. 5D). Moreover, the ability of USP13−C343A to promote the autophagic degradation of STING protein was also significantly reduced compared with USP13−WT (Fig. 5E and F). Taken together, USP13 regulates K63-linked deubiquitination of STING *via* its active site C343 and subsequently promotes the degradation of STING *via* P62-mediated autophagy (Fig. 5G).

3.6. USP13 attenuates Dox-induced cardiomyocyte death and inflammation via negatively regulating STING

STING mediates Dox-induced death, the abnormal activation of downstream TBK1, and inflammation in cardiomyocytes[16]. Thus, we examined the effects of USP13 on STING-related inflammatory response and death in Dox-challenged cardiomyocytes. As a hallmark of cell death, propidium iodide (PI) staining was employed to access membrane permeability. We observed that PI-positive nuclei were reduced in HL-1 cells overexpressing USP13 under Dox stress (Fig. 6A). Similarly, USP13^{oe} enhanced cell viability and decreased LDH release in cardiomyocytes under Dox stress (Fig. 6B). We also found that USP13 inhibited the phosphorylation of TBK1 in Dox-induced HL-1 cells (Fig. 6C), as well as the increased transcription of inflammatory genes *Tnf*, *Il6*, and *Ifnb1* (Fig. 6D). On the contrary, pharmacological inhibition of USP13 activity by Spautin-1 significantly intensified Dox-induced cardiomyocyte death (Fig. 6E and F), TBK1 activation (Fig. 6G) and inflammatory cytokine expression (Fig. 6H) in HL-1 cells. These results revealed that USP13 attenuates Dox-induced cardiomyocyte death and inflammation.

To verify the USP13−STING axis in Dox-induced cardiomyocyte death and inflammation, we constructed STING knockout (STINGKO) HL-1 cells and overexpressed USP13 in these cells. As expected, USP13^{oe} and STINGKO protected cardiomyocytes from Dox-induced cell death (Supporting Information Fig. S7A and S7B), TBK1 phosphorylation, and inflammatory gene expression (Fig. S7C and S7D). It's worth noting that USP13^{oe} failed to show more protective effects in STINGKO HL-1 cells with Dox challenge (Fig. S7). Taken together, USP13 protects cardiomyocytes against Dox-induced cell death and inflammation *via* STING.

3.7. USP13 negatively regulates Dox-induced STING activation and inflammation in vivo

Finally, we investigated the effects of USP13 on STING-related inflammation *in vivo*. Our findings revealed that overexpression of USP13 in cardiomyocytes reduced STING protein levels and STING/TBK1 activation (Fig. 7A and B) as well as the inflammatory cytokine expression (Fig. 7C) in Dox-challenged mouse heart tissues. Conversely, USP13CKO increased STING levels and aggravated the activation of STING and TBK1 (Fig. 7D and E), as well as inflammatory gene expression (Fig. 7F) in heart tissues of mice challenged with Dox. These findings highlight the critical role of USP13 in attenuating Dox-induced STING-related inflammation *in vivo*.

4. Discussion

Dox, as a commonly used chemotherapeutic drug, holds a dose-dependent heart toxicity, which restricts the clinical application of Dox[1,2]. Several DUBs have been reported to be involved in the regulation of DIC, including USP36, OTUD1, and OTUD7B. Dox treatment elevated the expression of USP36 in cardiomyocytes, and USP36 exacerbates the development of DIC *via* enhancing oxidative stress and cardiomyocyte apoptosis[9]. Recently, OTUD7B has been shown to prevent DIC by blocking autophagy and oxidative stress[30]. Our research team engaged in the regulation of DUBs in cardiovascular diseases. We have previously revealed that several DUBs are involved in the regulation of hypertensive cardiac hypertrophy and remodeling, such as USP25[18], YOD1[20], OTUD1[21], OTUD6a[23], and JOSD2[24]. In this study, through a comparison of transcriptomes and function screens, we identified USP13 as a potential regulator of DIC. We showed that cardiac-specific knockout of USP13 worsened Dox-induced cardiac dysfunction and injury. On the contrary, USP13 overexpression in cardiomyocytes ameliorated DIC. Given the specificity of USP13 in pathological cardiomyocytes, we believe that cardiomyocyte-targeted gene therapy of USP13, for example, AAVs encoding the cardiac-specific promoter (*cTNT* or *Myh6*) and *Usp13* gene, could be a potential therapeutic strategy for DIC.

DUBs perform their biological function by affecting the stability or function of their substrate proteins. USP13 functions as a DUB through different substrate proteins in different diseases[12,13]. Here, we conducted a Co-IP coupled LC−MS/MS analysis and identified that STING is a direct USP13 substrate protein in cardiomyocytes, which is consistent with a previous antiviral study[31]. STING is an important regulator for the innate immune response against pathogens by recruiting and activating TBK1, which subsequently raises the expression of inflammatory cytokines[15]. The critical roles of STING in myocardial ischemic injury[32], hypertrophy-associated heart failure[33], lipopolysaccharide-induced cardiac dysfunction[34], and DIC[16] have been recently

reported. Luo and colleagues[16] found that STING deficiency effectively reduced Dox-induced cardiac dysfunction. In addition to genetic inhibition, pharmacologically inhibiting STING by small-molecule C-176 has also been shown to protect against myocardial hypertrophy[35] and DIC[16], indicating that STING can be used as a therapeutic target for the treatment of DIC. However, STING is widely expressed and plays important roles in the pathophysiology of multiple organs[36]. Here, we found that USP13 is mainly expressed in cardiomyocytes and cardiomyocyte-specific USP13 deubiquitinates STING, subsequently alleviating cardiomyocyte death and inflammation induced by Dox. Therefore, we present that USP13 may be a more cardiomyocyte-specific target than STING for DIC treatment.

The ubiquitination of STING and its upstream E3 ligases and DUBs have been widely reported[37]. Interestingly, a previous study found that USP13 interacts with STING and promotes the deubiquitination of STING, thereby lessening the antiviral responses by decreasing the activation of STING−TBK1 signaling[31]. Here, we showed the interaction between STING and USP13 in cardiomyocytes during DIC, and the K63-linked deubiquitination of STING by USP13 resulted in the STING degradation *via* a P62-dependent autophagic way. K63-linked ubiquitin chain is one of the most prevalent forms of ubiquitination, which predominantly affects the activation and protein−protein interaction of substrate protein[7]. In general, DUBs inhibit proteasome-related degradation of substrate protein by removing ubiquitin molecules from the target protein. While some DUBs can also promote the degradation of substrate in an autophagy-dependent manner or other non-classical ways[38]. Our research revealed that USP13 inhibits the STING−TBK1 signaling by promoting autolysosome-related degradation of STING rather than the traditional proteolytic signaling paradigm. In 2018, Prabakaran and colleagues[26] found that P62, a selective autophagy receptor, interacted with STING to promote the degradation of STING through autophagy. Our data also suggest that USP13 promotes STING−P62 interaction and then leads to the autolysosome-related degradation of STING in a P62-dependent manner in cardiomyocytes. This is the first time to show a DUB negatively regulates STING stability *via* P62-mediated autophagy.

Our study still exists some potential limitations. In addition to STING, USP13 has also been reported to bind other potential substrate proteins[12,13], and USP13 might also affect the development of DIC through other substrates. Our scRNA-seq showed that USP13 is mainly distributed in cardiomyocytes, but USP13 is also expressed in non-cardiomyocytes, including macrophages, endothelial cells, and fibroblasts. It has been reported that USP13 expression in macrophages negatively regulates antiviral response[31]. Although we used cardiomyocyte-specific USP13 deficient or overexpressed mice to support our conclusion, we cannot completely rule out the involvement of non-cardiomyocyte USP13 in the regulation of DIC.

5. Conclusions

Cardiomyocyte-derived USP13 mitigates DIC. Mechanistically, USP13 deubiquitinates STING, thereby promoting its autolysosome-related degradation. This process subsequently alleviates cardiomyocyte inflammation and reduces cell death. Our study demonstrates that USP13 plays a cardioprotective role in DIC and highlights its potential as a therapeutic target for the treatment of DIC (Fig. 7G).

Acknowledgements

This study was supported by National Natural Science Foundation of China (82271347 to Gaojun Wu and U24A20814 to Guang Liang).

Author contributions

Liming Lin: Writing − original draft, Methodology, Investigation, Data curation. Jibo Han: Writing − original draft, Formal analysis, Data curation, Conceptualization. Diyun Xu: Investigation. Zimin Fang: Investigation. Bozhi Ye: Investigation. Jinfu Qian: Investigation. Xue Han: Data curation, Conceptualization. Julian Min: Conceptualization. Xiaohong Long: Visualization, Supervision, Resources, Funding acquisition. Gaojun Wu: Supervision, Resources, Project administration, Funding acquisition, Formal analysis, Conceptualization. Guang Liang: Visualization, Validation, Supervision, Resources, Project administration, Funding acquisition, Conceptualization.

Conflicts of interest

The authors declare no competing interests.

Appendix A. Supporting information

Supporting information to this article can be found online at https://doi.org/10.1016/j.apsb.2025.03.051.

References

1. Early Breast Cancer Trialists' Collaborative Group. Anthracycline-containing and taxane-containing chemotherapy for early-stage operable breast cancer: a patient-level meta-analysis of 100,000 women from 86 randomised trials. *Lancet* 2023;**401**:1277−92.
2. Wu L, Wang L, Du Y, Zhang Y, Ren J. Mitochondrial quality control mechanisms as therapeutic targets in doxorubicin-induced cardiotoxicity. *Trends Pharmacol Sci* 2023;**44**:34−49.
3. Yeh ET, Bickford CL. Cardiovascular complications of cancer therapy: incidence, pathogenesis, diagnosis, and management. *J Am Coll Cardiol* 2009;**53**:2231−47.
4. Christidi E, Brunham LR. Regulated cell death pathways in doxorubicin-induced cardiotoxicity. *Cell Death Dis* 2021;**12**:339.
5. Lipshultz SE, Nader R, Dalton VM, Levy DE, Silverman LB, Lipsitz SR, et al. The effect of dexrazoxane on myocardial injury in doxorubicin-treated children with acute lymphoblastic leukemia. *N Engl J Med* 2004;**351**:145−53.
6. Seif AE, Walker DM, Yimei L, Huang YSV, Marko K, Kari T, et al. Dexrazoxane exposure and risk of secondary acute myeloid leukemia in pediatric oncology patients. *Pediatr Blood Cancer* 2015;**62**:704−9.
7. Deng L, Meng T, Chen L, Wei W. The role of ubiquitination in tumorigenesis and targeted drug discovery. *Signal Transduct Targeted Ther* 2020;**5**:11.
8. Mevissen TET, Komander D. Mechanisms of deubiquitinase specificity and regulation. *Annu Rev Biochem* 2017;**86**:159−92.
9. Wang D, Jiang Z, Kan J, Jiang X, Pan C, You S, et al. USP36-mediated PARP1 deubiquitination in doxorubicin-induced cardiomyopathy. *Cell Signal* 2024;**117**:111070.
10. Xu F, Zang T, Chen H, Zhou C, Wang R, Yu Y, et al. Deubiquitinase OTUB1 regulates doxorubicin-induced cardiotoxicity *via* deubiquitinating c-MYC. *Cell Signal* 2024;**113**:110937.
11. Timms KM, Ansari-Lari MA, Morris W, Brown SN, Gibbs RA. The genomic organization of Isopeptidase T-3 (ISOT-3), a new member of the ubiquitin specific protease family (UBP). *Gene* 1998;**217**:101−6.

12. Wang Q, Sun Z, Xia W, Sun L, Du Y, Zhang Y, et al. Role of USP13 in physiology and diseases. *Front Mol Biosci* 2022;**9**:977122.
13. Li X, Yang G, Zhang W, Qin B, Ye Z, Shi H, et al. USP13: multiple functions and target inhibition. *Front Cell Dev Biol* 2022;**10**:875124.
14. Xu M, Tan J, Zhu L, Ge C, Dong W, Dai X, et al. The deubiquitinating enzyme 13 retards non-alcoholic steatohepatitis *via* blocking inactive rhomboid protein 2-dependent pathway. *Acta Pharm Sin B* 2023;**13**: 1071−92.
15. Ishikawa H, Barber GN. STING is an endoplasmic reticulum adaptor that facilitates innate immune signalling. *Nature* 2008;**455**:674−8.
16. Luo W, Zou X, Wang Y, Dong Z, Weng X, Pei Z, et al. Critical role of the cGAS−STING pathway in doxorubicin-induced cardiotoxicity. *Circ Res* 2023;**132**:e223−42.
17. Ye B, Shi X, Xu J, Dai S, Xu J, Fan X, et al. Gasdermin D mediates doxorubicin-induced cardiomyocyte pyroptosis and cardiotoxicity *via* directly binding to doxorubicin and changes in mitochondrial damage. *Transl Res* 2022;**248**:36−50.
18. Ye B, Zhou H, Chen Y, Luo W, Lin W, Zhao Y, et al. USP25 ameliorates pathological cardiac hypertrophy by stabilizing SERCA2a in cardiomyocytes. *Circ Res* 2023;**132**:465−80.
19. Xie S, Liu S, Zhang T, Shi W, Xing Y, Fang W, et al. USP28 serves as a key suppressor of mitochondrial morphofunctional defects and cardiac dysfunction in the diabetic heart. *Circulation* 2023;**149**:684−706.
20. Lin WT, Jiang YC, Mei YL, Chen YH, Zheng ZZ, Han X, et al. Endothelial deubiquinatase YOD1 mediates Ang II-induced vascular endothelial-mesenchymal transition and remodeling by regulating β-catenin. *Acta Pharmacol Sin* 2024;**45**:1618−31.
21. Wang M, Han X, Yu T, Wang M, Luo W, Zou C, et al. OTUD1 promotes pathological cardiac remodeling and heart failure by targeting STAT3 in cardiomyocytes. *Theranostics* 2023;**13**:2263−80.
22. Liu L, Pang J, Qin D, Li R, Zou D, Chi K, et al. Deubiquitinase OTUD5 as a novel protector against 4-HNE-triggered ferroptosis in myocardial ischemia/reperfusion injury. *Adv Sci (Weinh)* 2023;**10**: e2301852.
23. Fang Z, Han J, Lin L, Ye B, Qu X, Zhang Y, et al. Deubiquitinase OTUD6a drives cardiac inflammation and hypertrophy by deubiquitination of STING. *Biophys Acta Mol Basis Dis* 2024;**1870**:167061.
24. Han J, Fang Z, Han B, Ye B, Lin W, Jiang Y, et al. Deubiquitinase JOSD2 improves calcium handling and attenuates cardiac hypertrophy and dysfunction by stabilizing SERCA2a in cardiomyocytes. *Nat Cardiovasc Res* 2023;**2**:764−77.
25. Liu J, Xia H, Kim M, Xu L, Li Y, Zhang L, et al. Beclin1 controls the levels of p53 by regulating the deubiquitination activity of USP10 and USP13. *Cell* 2011;**147**:223−34.
26. Prabakaran T, Bodda C, Krapp C, Zhang BC, Christensen MH, Sun C, et al. Attenuation of cGAS−STING signaling is mediated by a p62/SQSTM1-dependent autophagy pathway activated by TBK1. *EMBO J* 2018;**37**:e97858.
27. Xiao D, Chang W, Ding W, Wang Y, Fa H, Wang J. Enhanced mitophagy mediated by the YAP/Parkin pathway protects against DOX-induced cardiotoxicity. *Toxicol Lett* 2020;**330**:96−107.
28. Zhang YH, Zhou CJ, Zhou ZR, Song AX, Hu HY. Domain analysis reveals that a deubiquitinating enzyme USP13 performs non-activating catalysis for Lys63-linked polyubiquitin. *PLoS One* 2011;**6**:e29362.
29. Zhao X, Fiske B, Kawakami A, Li J, Fisher DE. Regulation of MITF stability by the USP13 deubiquitinase. *Nat Commun* 2011;**2**:414.
30. Zhang J, Zha Y, Jiao Y, Li Y, Zhang S. Protective role of cezanne in doxorubicin-induced cardiotoxicity by inhibiting autophagy, apoptosis and oxidative stress. *Toxicology* 2023;**485**:153426.
31. Sun H, Zhang Q, Jing YY, Zhang M, Wang HY, Cai Z, et al. USP13 negatively regulates antiviral responses by deubiquitinating STING. *Nat Commun* 2017;**8**:15534.
32. Cao D, Schiattarella GG, Villalobos E, Jiang N, May HI, Li T, et al. Cytosolic DNA sensing promotes macrophage transformation and governs myocardial ischemic injury. *Circulation* 2018;**137**: 2613−34.
33. Han J, Dai S, Zhong L, Shi X, Fan X, Zhong X, et al. GSDMD (Gasdermin D) mediates pathological cardiac hypertrophy and generates a feed-forward amplification cascade *via* mitochondria-STING (stimulator of interferon genes) axis. *Hypertension* 2022;**79**:2505−18.
34. Li N, Zhou H, Wu H, Wu Q, Duan M, Deng W, et al. STING−IRF3 contributes to lipopolysaccharide-induced cardiac dysfunction, inflammation, apoptosis and pyroptosis by activating NLRP3. *Redox Biol* 2019;**24**:101215.
35. Wang L, Zhang S, Liu H, Gao L, He L, Chen Y, et al. STING activation in cardiomyocytes drives hypertrophy-associated heart failure *via* NF-κB-mediated inflammatory response. *Biochim Biophys Acta, Mol Basis Dis* 2024;**1870**:166997.
36. Motwani M, Pesiridis S, Fitzgerald KA. DNA sensing by the cGAS−STING pathway in health and disease. *Nat Rev Genet* 2019; **20**:657−74.
37. Jiang W, Li M, Peng S, Hu T, Long Y, Zhang J, et al. Ubiquitin ligase enzymes and de-ubiquitinating enzymes regulate innate immunity in the TLR, NLR, RLR, and cGAS−STING pathways. *Immunol Res* 2023;**71**:800−13.
38. Xie W, Tian S, Yang J, Cai S, Jin S, Zhou T, et al. OTUD7B deubiquitinates SQSTM1/p62 and promotes IRF3 degradation to regulate antiviral immunity. *Autophagy* 2022;**18**:2288−302.